

Winding Berry dipole on uniaxially strained graphene/hBN/hBN moiré trilayers

Angiolo Huamán^{1,*} and Salvador Barraza-Lopez^{1,†}

¹*Department of Physics, University of Arkansas, Fayetteville, Arkansas 72701, USA and MonArk NSF Quantum Foundry, University of Arkansas, Fayetteville, Arkansas 72701, USA*

(Dated: December 17, 2024)

Nonlinear Hall-like currents can be generated by a time-periodic alternating bias on two-dimensional (2D) materials lacking inversion symmetry. To hint that the moiré between graphene and its supporting substrate contributes to the homogeneity of nonlinear currents, the change in the local potential $\Delta V(\mathbf{r})$ around horizontally strained graphene due to a homobilayer of hexagonal boron nitride (hBN) was obtained from *ab initio* calculations, and corrections to on-site energies and hopping matrix elements on graphene's tight-binding electronic dispersion of π -electrons were calculated. Relying on a semiclassical approximation, Berry dipoles \mathbf{D} are seen to change orientation and wind throughout the moiré.

Nonlinear Hall-effects can originate from Berry dipoles \mathbf{D} in materials with broken spatial inversion symmetry. In gapped graphene with anisotropic Fermi velocities v_x and v_y , \mathbf{D} can be created by the tilting of gapped Dirac cones [1]:

$$H_1 = \hbar(v_x k_x \sigma_x + \xi v_y k_y \sigma_y) + \frac{\Delta}{2} \sigma_z + \xi \alpha k_y \quad (1)$$

(where ξ is the valley degree of freedom, Δ is the electronic band gap, σ_x , σ_y and σ_z are Pauli matrices, and α is a parameter characterizing the tilt), or by band warping [2]:

$$H_2 = \hbar(v_x k_x \sigma_x + \xi v_y k_y \sigma_y) + \frac{\Delta}{2} \sigma_z + (\lambda_1 k_x^2 - \lambda_2 k_y^2) \sigma_x + 2\xi \lambda_3 k_x k_y \sigma_y \quad (2)$$

through nonzero inverse masses λ_j/\hbar^2 ($j = 1, 2, 3$). The Berry dipole is the integral of the \mathbf{k} -derivatives of the Berry curvature $\Omega_z^{(n)}$ [3] over the first Brillouin zone (1BZ), weighted by the Fermi-Dirac distribution f_0 at chemical potential μ [4]:

$$\mathbf{D}(\mu) = \int_{\text{1BZ}} d^2k \sum_n f_0(\epsilon_n(\mathbf{k}), \mu) \nabla_{\mathbf{k}} \Omega_z^{(n)}, \quad (3)$$

where n runs over all bands and $d^2k = dk_x dk_y$ implies a two-dimensional integral in reciprocal space. The relation between \mathbf{D} and nonlinear (quadratic) currents was established in the semiclassical regime and in the relaxation time approximation [1]. When the bias has a frequency ω , the second-order alternating current with frequency 2ω is $[j_{2\omega}^{(2)}]_i = \sigma_{ijk} \mathcal{E}_j \mathcal{E}_k$, where the second order conductivity tensor σ_{ijk} only has two nonzero independent components:

$$\sigma_{yxx} = \frac{e^3 \tau}{2\hbar^2} \frac{D_x}{1 + i\omega\tau}, \quad \text{and} \quad \sigma_{xyy} = \frac{e^3 \tau}{2\hbar^2} \frac{D_y}{1 + i\omega\tau}, \quad (4)$$

with τ the electron relaxation time. This Berry dipole induces a *transversal* (i.e., normal to the bias field) second order

current in Hall bar setups [5], and its direction is fixed once parameters v_x , v_y , Δ , α , λ_1 , λ_2 , and λ_3 are set. Other sources of second order current (skew scattering and side jump processes [6]) are invoked to produce a *longitudinal* nonlinear current, parallel to the direction in which the bias is applied, and thus *homogenize the nonlinear current*. The question addressed in this Letter is *whether other (quantum, topological) mechanisms exist to generate transverse and longitudinal currents on graphene in ultra-pure samples, and the answer is in the affirmative if parameters $v_{x,y}$, Δ , α and λ_j are spatially modulated within a moiré*.

In reaching that conclusion, the main assumption made is that constructing \mathbf{D} as a local vector field makes sense. Detailed discussions of the effect of local strain and twist angle on graphene/hBN monolayers indicate the presence of locally slowly varying (i.e., *semiclassical*) (i) mass terms $m(\mathbf{r})$ (that is, energy gaps) and (ii) strain fields $\mathbf{A}(\mathbf{r})$ [7], the latter can be interpreted as a local anisotropy in the nearest neighbor hopping integrals. Additionally, a gapped Dirac dispersion for the entire moiré supercell is found at energies ± 0.1 eV within the Fermi energy (the band gap is of the order of 10 meV [7]).

Moirés can be created by a relative rotation of two homobilayers, by homogeneously straining one monolayer with respect to the other one, or by shear [8]. Moirés lead to the formation of domains and domain walls [8]. Winding magnetic and electric polar fields have been reported in moirés created on homobilayers by a relative rotation [9, 10]. Consistent with Ref. [7], a moiré supercell with a lattice parameter of 136.4 Å and no relative twist angle is being considered here. This moiré is of the “homogeneous strain” type, which occurs naturally on heterobilayers. This type of moiré features on a study of light-induced shift currents in WSe₂/WS₂ superlattices [11], and in a discussion of the ferroelectric order in graphene/MoTe₂ heterostructures [12].

As shown by Engelke *et al.* [13], moirés can be thought of as collections of *local registries among two lattices*; this collection of local registries is the parameter space at hand here [14]. Determining \mathbf{D} at each point on this parameter space, and then placing \mathbf{D} back onto the moiré, a “slowly varying” $\mathbf{D}(\mathbf{r})$ is obtained, in the same way as semiclassical approximations such as “strain engineering of graphene” [15].

We studied graphene on a AB (polar) hBN bilayer substrate.

* ah200@uark.edu

† sbarraza@uark.edu

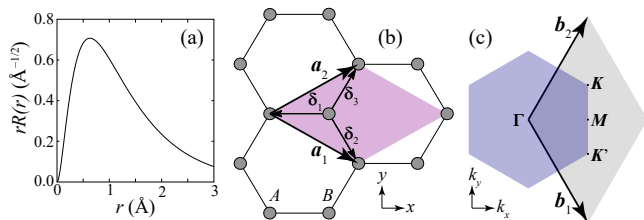


FIG. 1. (a) Radial part (times r) of the carbon atomic orbital $\phi_z(\mathbf{r})$ used to calculate matrix elements in Eqn. (5). (b) Graphene's lattice vectors $\mathbf{a}_{1,2} = a_{0,g}(\sqrt{3}, \mp 1)/2$ and first nearest neighbor vectors δ_j ($j = 1, 2, 3$). (c) Hexagonal first Brillouin zone, showing the $\Gamma = \mathbf{0}$, $\mathbf{M} = (\mathbf{b}_1 + \mathbf{b}_2)/2$, $\mathbf{K} = (\mathbf{b}_1 + 2\mathbf{b}_2)/3$, and $\mathbf{K}' = (2\mathbf{b}_1 + \mathbf{b}_2)/3$ high-symmetry points.

Working in parameter space [13], the changes to the on-site energies and first nearest neighbor hopping terms due to the electrostatic disturbance $\Delta V(\mathbf{r})$ created by a proximal polar (AB) hBN homobilayer substrate were calculated first, and a single unit cell graphene Hamiltonian having those local changes was next constructed from which $\mathbf{D}(\mathbf{r})$ is evaluated (in parameter space, a local commensuration is set such that the hBN bilayer takes graphene's lattice parameter once a local registry between the two materials is found). The different registries between graphene and the AB hBN substrate at varying locations within the moiré give rise to local potential profiles that determine $\mathbf{D}(\mathbf{r})$.

To calculate the effective potential $\Delta V(\mathbf{r})$, as well as to optimize atomistic structures, the *ab initio* VASP code [16–18] was employed with the generalized gradient approximation (GGA) for exchange-correlation (xc) as implemented by Perdew, Burke and Ernzerhof (PBE) [19], and van der Waals modifications due to Klimeš and coworkers [20, 21]. The energy cut-off was set to 600 eV, and the number of k -points was $16 \times 16 \times 1$. The lattice constant along the z -direction was set to $|c| = c = 40 \text{ \AA}$. The structures were made commensurate, and subsequently elongated along the horizontal (x) direction by 0.5%. This elongation breaks threefold symmetry and it is one ingredient for the creation of Berry dipoles [22]. The optimal height between graphene and the AB hBN substrate bilayer was obtained by minimizing the heterostructure's total energy while vertically displacing graphene, with the homobilayer coordinates kept fixed. Graphene's in-plane coordinates were fixed throughout this optimization.

The *change* in local potential around graphene due to the AB hBN bilayer substrate, which will give rise to $\mathbf{D}(\mathbf{r})$, was obtained from the total potential of a vertical heterostructure [$V_{total}(\mathbf{r})$], and the local potential of each of its three integrating monolayers: [graphene, $V_g(\mathbf{r})$], and two hBN monolayers [$V_{subs1}(\mathbf{r})$ and $V_{subs2}(\mathbf{r})$] by removal of the other two monolayers, without modifying the atomic positions of the remaining one. Specifically, $\Delta V(\mathbf{r}) = V_{total}(\mathbf{r}) - V_g(\mathbf{r}) - V_{subs1}(\mathbf{r}) - V_{subs2}(\mathbf{r})$. (Although an hBN bilayer was used in this work, similar results may be obtained when calculations involve graphene and other substrates.)

In a tight-binding description of graphene's π -electrons, first-nearest neighbor hopping elements get normalized by the

TABLE I. Structural information.

$(a_{sub}/a_0, a_g/a_0, g)$	(1,1)	(54,55)
$\frac{a_{sub}-a_g}{a_g} \times 100$	1.800	-0.030
N_{atoms}	6	17 714
N_C	2	6050

AB hBN substate as $t_{ij} = t + \Delta t_{ij}$ ($t = -2.83 \text{ eV}$ [23]), with:

$$\Delta t_{ij} = \int d^3\mathbf{r} \phi_z(\mathbf{r} - \mathbf{R}_j) \Delta V(\mathbf{r}) \phi_z(\mathbf{r} - \mathbf{R}_i), \quad (5)$$

where \mathbf{R}_i and \mathbf{R}_j are the positions of two carbon first-nearest neighbors, and $1 \leq i, j \leq N_C$. The radial part of the real function $\phi_z(\mathbf{r})$, taken from the ATOM code [24, 25], is provided in Fig. 1(a). On-site energies within a unit cell [shaded region in Fig. 1(b)], ϵ_A and ϵ_B , are integrals for which $\mathbf{R}_i = \mathbf{R}_j$. This gives a graphene unit cell Hamiltonian with on-site energies ϵ_A and ϵ_B , with an energy gap $\Delta E = \epsilon_A - \epsilon_B$ and anisotropic nearest-neighbor hoppings t_j ($j = 1, 2, 3$), corresponding to the three first nearest neighbor bonds δ_j ($j = 1, 2, 3$) shown in Fig. 1(b). Figure 1(c) contains the hexagonal 1BZ (shaded purple) as well as reciprocal lattice vector \mathbf{b}_j ($j = 1, 2$) and a primitive unit cell (shaded gray).

The tight-binding Hamiltonian obtained with the renormalized matrix elements from Eqn. (5) was used to calculate \mathbf{D} [Eqn. (3)] numerically, which requires determining the Berry curvature [3]. The Gauss-Legendre quadrature was used for integration in a region of reciprocal space where the Berry curvature is the largest.

Graphene's optimized lattice parameter is $a_{0,g} = 2.471 \text{ \AA}$, and that of hBN is $a_0 = 2.516 \text{ \AA}$. The first row of Table I contains normalized supercell sizes, written down in terms of the hBN lattice parameter a_0 (first entry), or graphene's lattice constant $a_{0,g}$ (second entry). The first one, dubbed (1,1), only requires six atoms. The (54,55) one is large enough to study the in-plane distribution of \mathbf{D} within a moiré. As shown in the second row of the table, the hBN lattice parameter was compressed or elongated to guarantee commensuration. Rows three and four in Table I contain the total number of atoms N_{atoms} and the number of carbon atoms N_C , respectively. The optimal separation between graphene and the uppermost substrate layer was 3.39 \AA .

Highly symmetric stacking configurations *ABA* and *ABC* can be found in the (54,55) supercell [Fig. 2]. Nomenclature is introduced now: let \mathbf{a}_1 and \mathbf{a}_2 be the lattice vectors shown in Fig. 1(b). The hBN monolayer with an *A* configuration will be defined as the one in which the nitrogen (N) atoms lie at the common origin of \mathbf{a}_1 and \mathbf{a}_2 (and at the ends of these lattice vectors), while the boron (B) atoms are at the additional corners. Dating back to Bernal [26], the relative stacking of non-turbostatic graphite is such that even layers are displaced by $(\mathbf{a}_1 + \mathbf{a}_2)/3$, on the periodically repeating stacking sequence dubbed *AB*; the stacking sequence is understood to be ordered from bottom to top. Graphite obtained from a diamond configuration has three monolayers periodically repeating; the second (third) one is horizontally displaced by $(\mathbf{a}_1 + \mathbf{a}_2)/3$ [$2(\mathbf{a}_1 + \mathbf{a}_2)/3$] with respect to

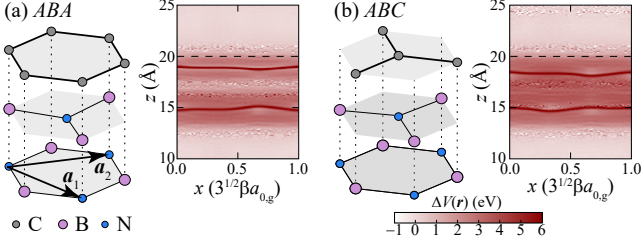


FIG. 2. (a) *ABA* and (b) *ABC* stacked graphene/hBN homobilayer heterojunctions and effective potential $\Delta V(\mathbf{r})$ (using the same scale for both subplots). The position of graphene ($z = 20 \text{ \AA}$) is indicated by horizontal dashed lines.

the bottommost one; this stacking configuration is known as *ABC*. The stacking labeling convention described in this paragraph was employed in Fig. 2.

Next to each stacking diagram in Fig. 2 there are side views of the corresponding effective potential $\Delta V(\mathbf{r})$. These are cuts along the longest diagonal (*i.e.*, parallel to the plane spanned by $\mathbf{a} + \mathbf{b}$ and \mathbf{c}), with $\mathbf{a} = a_g(\sqrt{3}\beta, -1)/2$, $\mathbf{b} = a_g(\sqrt{3}\beta, 1)/2$ ($\beta = 1.005$ because of the longitudinal strain applied), and $\mathbf{c} = (0, 0, c)$. The z range is just a vicinity of the graphene position, which is indicated by a horizontal dashed line at $z = 20 \text{ \AA}$. These plots show the inhomogeneities that lead to $\epsilon_A \neq \epsilon_B$ and to anisotropic hopping parameters t_j . A slowly spatially varying (*e.g.*, semiclassical) graphene Hamiltonian was constructed using the on-site energies and hopping parameters defined in Eqn. (5):

$$H = \sum_{\mathbf{k}, s=A,B} \epsilon_s c_{\mathbf{k}s}^\dagger c_{\mathbf{k}s} + \sum_{\mathbf{k}} [f(\mathbf{k}) c_{\mathbf{k}A}^\dagger c_{\mathbf{k}B} + \text{h.c.}], \quad (6)$$

with $f(\mathbf{k}) = t + \Delta t_3 + (t + \Delta t_1)e^{-i\mathbf{k}\cdot\mathbf{a}_1} + (t + \Delta t_2)e^{-i\mathbf{k}\cdot\mathbf{a}_2}$ and $c_{\mathbf{k}A,B}$ annihilation operators.

The Cartesian components of the Berry dipole $\mathbf{D} = (D_x, D_y)$ are shown in Fig. 3 for both the *ABA* and *ABC* heterostructures. D_x is zero because of the only mirror symmetry available $y \rightarrow -y$ [27, 28]. In addition, $t_1 < t_2 = t_3$ in both subplots. The D_y component accumulates just outside of the energy gap, reaching an absolute maximum of around 1 \AA , *i.e.*, of the same order of magnitude as that found in few-layer WTe₂ [29]. The direction of D_y can be tuned by the sign of the mass [1] (The temperature used for f_0 was 10^{-6} K .)

But can \mathbf{D} tilt as well? *i.e.*, can it have nonzero x and y components? To address this question, Fig. 4 shows color maps of the Berry curvature for unit cell Hamiltonians [Eqn. (6)] with elements Δt_j modified one at a time. (A coarser k -point grid can be employed when $|\Delta E| = |\epsilon_A - \epsilon_B|$ is large, and $\Delta E = -0.5 \text{ eV}$ was used in Fig. 4 for this reason). Setting the $(0,0)$ point in all subplots of Fig. 4 to correspond with the location of shifted the K -point, the Berry curvature is seen to accumulate *above or below* K [Figs. 4(a) and 4(b)] depending on whether $t_1 > t_2 = t_3$ or $t_1 < t_2 = t_3$, respectively. Similarly, the Berry curvature has an axis of symmetry at either -30° or 150° when $t_2 \neq t_1 = t_3$ [Figs. 4(c) and 4(d), respectively], or at 30° and 210° when

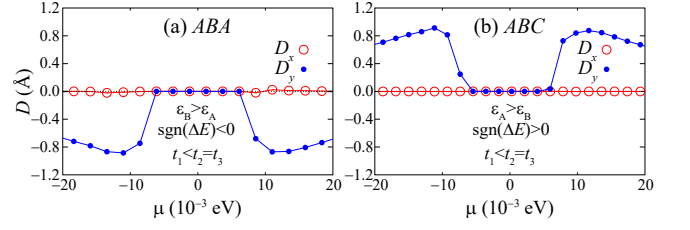


FIG. 3. Berry dipole \mathbf{D} for the *ABA* and *ABC* graphene/hBN homobilayer heterostructures as a function of the chemical potential μ . Mirror symmetry yields $D_x = 0$, and the sign of the gap determines the sign (direction) of D_y . The zero of μ was set at the center of the gap.

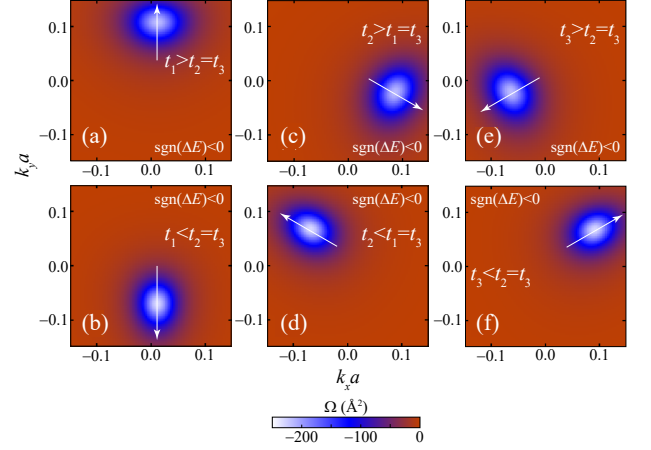


FIG. 4. Berry curvature for the valence band around the K valley. $\epsilon_B > \epsilon_A$ in all subplots. (a) $t_2 = t_3 = t$ and $t_1 = t + 0.5 \text{ eV}$, (b) $t_2 = t_3 = t$ and $t_1 = t - 0.5 \text{ eV}$, (c) $t_1 = t_3 = t$ and $t_2 = t + 0.5 \text{ eV}$, (d) $t_1 = t_3 = t$ and $t_2 = t - 0.5 \text{ eV}$, (e) $t_1 = t_2 = t$ and $t_3 = t + 0.5 \text{ eV}$ and (f) $t_1 = t_2 = t$ and $t_3 = t - 0.5 \text{ eV}$.

$t_3 \neq t_1 = t_2$ [Figs. 4(e) and 4(f)]. Additional and slight asymmetries in the hoppings t_j barely distort this picture, and so this will imply that the direction of $\mathbf{D} = (D_x, D_y)$ only has six possibilities, namely forming $\pm 90^\circ$, $\pm 30^\circ$ and $\pm 150^\circ$ angles with respect to the x -direction, thus reflecting a *trigonal-like symmetry constraint* [13].

This winding features in moirés: to show this, \mathbf{D} was calculated at 82 locations not related by symmetry, within the moiré depicted in Fig. 5(a). (This sampling is much smaller than the one used in Ref. [9] for another vector field, but calculations are much more time consuming here.) In doing so, one assumes the relative displacement to hold over a few neighboring unit cells, such that the assumption of periodicity holds; this is the semiclassical approximation alluded to at the beginning. Only graphene and the uppermost hBN monolayer are shown on Fig. 5(a) for clarity.

Within the moiré, the relative position of the graphene on top is such that the local stacking is *ABB* at the four corners of the moiré unit cell. Apart from the vertices, this moiré supercell exhibits highly symmetric regions with a well defined stacking: The centers of the two triangular halves have a *ABA* and *ABC* stacking [open and filled circles in Fig. 5(a),

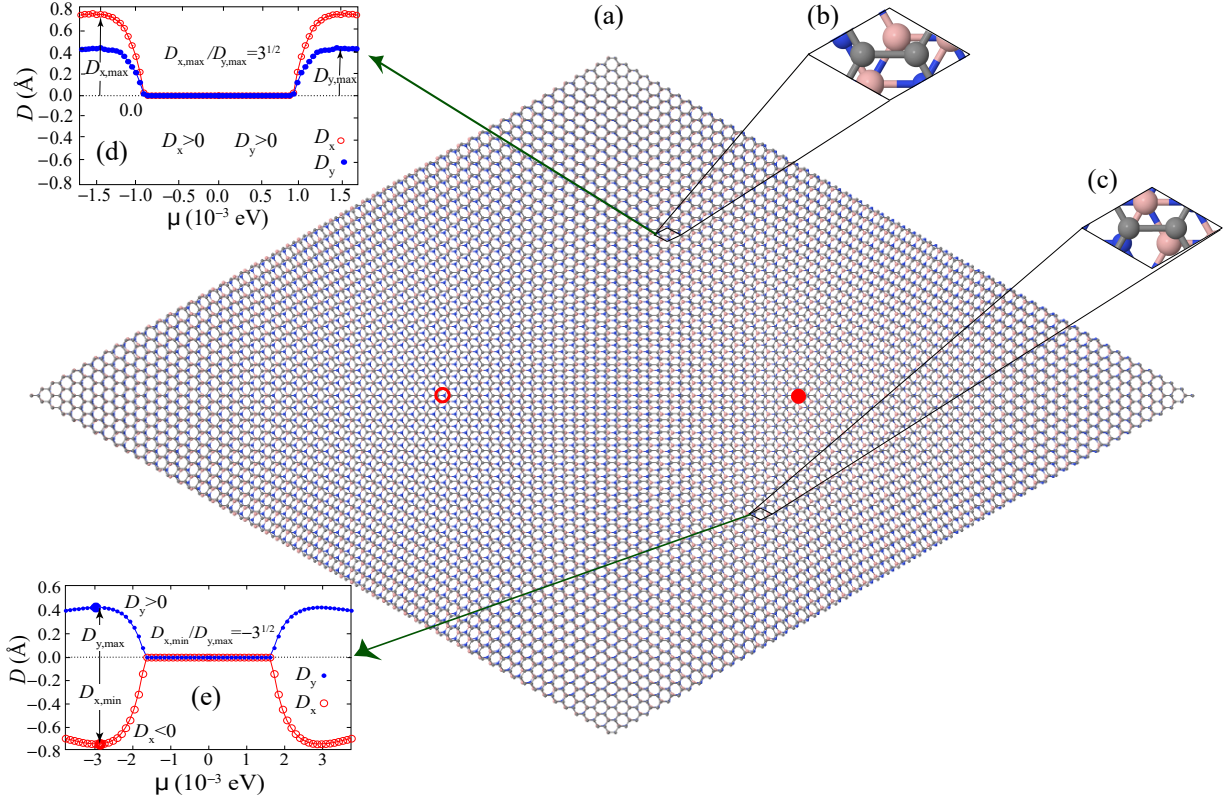


FIG. 5. (a) Moiré supercell of a $(54, 55)$ graphene/hBN homobilayer heterostructure. Only the upper hBN monolayer is shown for clarity. *ABA* and *ABC* configurations are highlighted by an open or closed circle, respectively. (b) and (c): two local cells yielding Berry dipoles with (d) $D_x > 0$ and $D_y > 0$ or (e) $D_x < 0$ and $D_y > 0$.

respectively], whose vectors \mathbf{D} were reported in Fig. 3.

Two additional registries are displayed within the moiré on Fig. 5(a); their unit cells display the asymmetric stacking shown on Figs. 5(b) and 5(c). Their corresponding \mathbf{D} are shown on Figs. 5(d) and 5(e), respectively. Different from Fig. 3, the two components of \mathbf{D} are now different from zero.

An interplay between the mass terms $\epsilon_A - \epsilon_B$ and the anisotropy of the hopping integrals t_j ($j = 1, 2, 3$) what ultimately leads to the *tilting* of the Berry dipole \mathbf{D} observed in Figs. 5(d) and 5(e). To see this, Fig. 6(a) maps the relative local displacements between graphene and the closest hBN unit cell atoms at the cell below (these vectors are defined between the centers of the corresponding local cells) for 82 registries within the moiré not related by symmetry. Solid lines on Fig. 6 encompass the confines of the moiré; the vertical line was drawn to highlight symmetries. Similarly, two open circles on all subplots of this Figure highlight *ABA* and *ABC* local configurations.

Figure 6(b) depicts a similar map for the onsite energy difference $\epsilon_A - \epsilon_B$; there is mass inversion across the solid lines indicated within the subplot as one moves away from the four edges of the moiré. (Since those edges feature an *ABB* stacking, they all induce a staggered potential with the same sign in graphene.) This mass inversion is akin to the topological helical modes found theoretically [30,

31] and experimentally [32] along domain walls in twisted bilayer graphene (which are rooted in the opposite valley Chern number on both side of the *AB* and *BA* domains). Figure 6(c) is a map of the direction of the maximum hopping parameter along the directions δ_j in Fig. 1(b). Although the actual functional dependence is not straightforward, the renormalized hopping terms Δt_j are related to the displacements shown in Fig. 6(a).

The winding vector map of \mathbf{D} is shown in Fig. 6(d) and this is the main result of this work. It establishes that moirés provide an additional knob for current homogenization and scattering and it opens the possibility of longitudinal (as well of transversal) second order currents *based solely on the Berry dipole*, even in ultraclean samples.

To summarize, a scheme for obtaining a nonzero Berry dipole of graphene on hBN homobilayer substrates was presented. When applied to a moiré supercell, a local distribution of the Berry dipole along six specific directions was obtained, which exhibits winding around highly symmetric points, and signals the possibility of having a second order longitudinal currents due to the local tilting of \mathbf{D} within the (inevitable) moirés created between graphene and any substrate, and a subsequent scattering that was not calculated here.

This work originated from conversations with Y. Liu

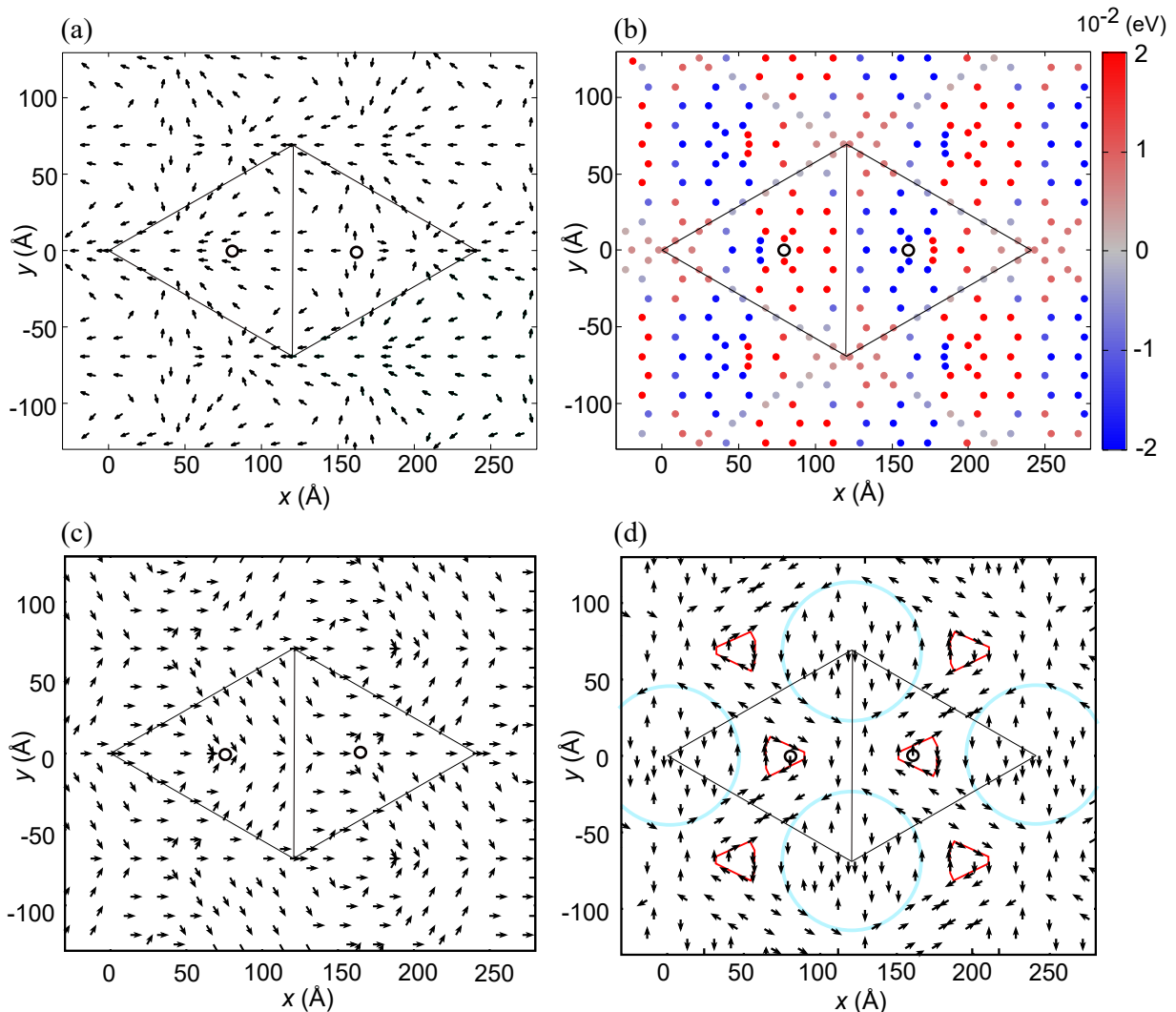


FIG. 6. (a) Relative displacement between the graphene unit cells and the closest hBN ones, for over 82 local registries within the moiré. (b) Onsite energy differences $[\epsilon_A - \epsilon_B]$, according to Fig. 1(b)) throughout the moiré. (c) Vector flow of the direction of the bond with the maximum value of the nearest neighbor hopping. (d) Local distribution of D .

and J. C. Hone. The authors thank S. P. Poudel and Hannah Isbell for technical assistance, and J. Van Horn-Morris for discussions. Calculations were performed on the Pinnacle Supercomputer, funded by the NSF

under award OAC-2346752. Financial support from the NSF's Q-AMASE-i program (Award DMR-1906383) is acknowledged.

-
- [1] I. Sodemann and L. Fu, Quantum nonlinear Hall effect induced by Berry curvature dipole in time-reversal invariant materials, *Phys. Rev. Lett.* **115**, 216806 (2015).
 [2] R. Battilomo, N. Scopigno, and C. Ortix, Berry curvature dipole in strained graphene: a Fermi surface warping effect, *Phys. Rev. Lett.* **123**, 196403 (2019).
 [3] D. Xiao, M.-C. Chang, and Q. Niu, Berry phase effects on electronic properties, *Rev. Mod. Phys.* **82**, 1959 (2010).
 [4] C.-P. Zhang, J. Xiao, B. T. Zhou, J.-X. Hu, Y.-M. Xie, B. Yan, and K. T. Law, Giant nonlinear Hall effect in strained twisted

- bilayer graphene, *Phys. Rev. B* **106**, L041111 (2022).
 [5] P. He, G. K. W. Koon, H. Isobe, J. Y. Tan, J. Hu, A. H. C. Neto, L. Fu, and H. Yang, Graphene moiré superlattices with giant quantum nonlinearity of chiral Bloch electrons, *Nat. Nanotechnol.* **17**, 378 (2022).
 [6] Z. Z. Du, H.-Z. Lu, and X. C. Xie, Nonlinear Hall effects, *Nat. Rev. Phys.* **3**, 744 (2021).
 [7] J. Jung, E. Laksono, A. M. DaSilva, A. H. MacDonald, M. Mucha-Kruczyński, and S. Adam, Moiré band model and band gaps of graphene on hexagonal boron nitride, *Phys. Rev.*

- B **96**, 085442 (2017).
- [8] P. Cazeaux, D. Clark, R. Engelke, P. Kim, and M. Luskin, Relaxation and domain wall structure of bilayer moiré systems, *J. Elast.* **154**, 443 (2023).
- [9] D. Bennett, G. Chaudhary, R. J. Slager, E. Bousquet, and P. Ghosez, Polar meron-antimeron networks in strained and twisted bilayers, *Nat. Commun.* **14**, 1629 (2023).
- [10] S. Li, Z. Sun, N. J. McLaughlin, A. Sharmin, N. Agarwal, M. Huang, S. H. Sung, H. Lu, S. Yan, H. Lei, R. Hovden, H. Wang, H. Chen, L. Zhao, and C. R. Du, Observation of stacking engineered magnetic phase transitions within moiré supercells of twisted van der Waals magnets, *Nat. Commun.* **15**, 5712 (2024).
- [11] C. Hu, M. H. Naik, Y.-H. Chan, J. Ruan, and S. G. Louie, Light-induced shift current vortex crystals in moiré heterobilayers, *Proc. Natl. Acad. Sci. U.S.A.* **120**, e2314775120 (2023).
- [12] A. O. Fumega and J. L. Lado, Ferroelectric valley valves with graphene/moTe₂ van der waals heterostructures, *Nanoscale* **15**, 2181 (2023).
- [13] R. Engelke, H. Yoo, S. Carr, K. Xu, P. Cazeaux, R. Allen, A. M. Valdivia, M. Luskin, E. Kaxiras, M. Kim, J. H. Han, and P. Kim, Topological nature of dislocation networks in two-dimensional moiré materials, *Phys. Rev. B* **107**, 125413 (2023).
- [14] J. P. Sethna, *Statistical Mechanics: Entropy, Order Parameters, and Complexity*, 1st ed. (Oxford U. Press, Oxford, U.K., 2006).
- [15] G. G. Naumis, S. Barraza-Lopez, M. Oliva-Leyva, and H. Terrones, Electronic and optical properties of strained graphene and other strained 2D materials: a review, *Rep. Prog. Phys.* **80**, 096501 (2017).
- [16] G. Kresse and J. Furthmüller, Efficient iterative schemes for *ab initio* total-energy calculations using a plane-wave basis set, *Phys. Rev. B* **54**, 11169 (1996).
- [17] G. Kresse and J. Furthmüller, Efficiency of *ab initio* total energy calculations for metals and semiconductors using a plane-wave basis set, *Comput. Mater. Sci.* **6**, 15 (1996).
- [18] G. Kresse and D. Joubert, From ultrasoft pseudopotentials to the projector augmented-wave method, *Phys. Rev. B* **59**, 1758 (1999).
- [19] J. P. Perdew, K. Burke, and M. Ernzerhof, Generalized gradient approximation made simple, *Phys. Rev. Lett.* **77**, 3865 (1996).
- [20] J. c. v. Klimeš, D. R. Bowler, and A. Michaelides, Van der Waals density functionals applied to solids, *Phys. Rev. B* **83**, 195131 (2011).
- [21] J. Klimeš, D. R. Bowler, and A. Michaelides, Chemical accuracy for the van der Waals density functional, *J. Phys.: Condens. Matter* **22**, 022201 (2009).
- [22] S. Sinha, P. C. Adak, A. Chakraborty, K. Das, K. Debnath, L. D. V. Sangani, K. Watanabe, T. Taniguchi, U. V. Waghmare, A. Agarwal, and M. M. Deshmukh, Berry curvature dipole senses topological transition in a moiré superlattice, *Nat. Phys.* **18**, 765 (2022).
- [23] A. H. Castro Neto, F. Guinea, N. M. R. Peres, K. S. Novoselov, and A. K. Geim, The electronic properties of graphene, *Rev. Mod. Phys.* **81**, 109 (2009).
- [24] R. W. Jansen and O. F. Sankey, *Ab initio* linear combination of pseudo-atomic-orbital scheme for the electronic properties of semiconductors: results for ten materials, *Phys. Rev. B* **36**, 6520 (1987).
- [25] O. F. Sankey and D. J. Niklewski, *Ab initio* multicenter tight-binding model for molecular-dynamics simulations and other applications in covalent systems, *Phys. Rev. B* **40**, 3979 (1989).
- [26] J. D. Bernal, The structure of graphite, *Proc. R. Soc. Lond. A* **106**, 749 (1924).
- [27] Q. Ma, S.-Y. Xu, H. Shen, D. MacNeill, V. Fatemi, T.-R. Chang, A. M. Mier Valdivia, S. Wu, Z. Du, C.-H. Hsu, S. Fang, Q. D. Gibson, K. Watanabe, T. Taniguchi, R. J. Cava, E. Kaxiras, H.-Z. Lu, H. Lin, L. Fu, N. Gedik, and P. Jarillo-Herrero, Observation of the nonlinear Hall effect under time-reversal-symmetric conditions, *Nature* **565**, 337 (2019).
- [28] S.-Y. Xu, Q. Ma, H. Shen, V. Fatemi, S. Wu, T.-R. Chang, G. Chang, A. M. M. Valdivia, C.-K. Chan, Q. D. Gibson, J. Zhou, Z. Liu, K. Watanabe, T. Taniguchi, H. Lin, R. J. Cava, L. Fu, N. Gedik, and P. Jarillo-Herrero, Electrically switchable Berry curvature dipole in the monolayer topological insulator WTe₂, *Nat. Phys.* **14**, 900 (2018).
- [29] K. Kang, T. Li, E. Sohn, J. Shan, and K. F. Mak, Nonlinear anomalous Hall effect in few-layer WTe₂, *Nat. Mater.* **18**, 324 (2019).
- [30] D. K. Efimkin and A. H. MacDonald, Helical network model for twisted bilayer graphene, *Phys. Rev. B* **98**, 035404 (2018).
- [31] F. Zhang, A. H. MacDonald, and E. J. Mele, Valley chern numbers and boundary modes in gapped bilayer graphene, *Proc. Natl. Acad. Sci. U.S.A.* **110**, 10546 (2013).
- [32] J. D. Verbakel, Q. Yao, K. Sotthewes, and H. J. W. Zandvliet, Valley-protected one-dimensional states in small-angle twisted bilayer graphene, *Phys. Rev. B* **103**, 165134 (2021).